machines

MDPI

Article

Preload-Loss State Identification of Bolted Joints Using Multi-Sensor Electromechanical Impedance Signals and a Distance-Weighted Graph Convolutional Network

Lu Li [1], Xingyu Fan [1,2,*], Yuxuan Wang [1], Tong Zhao [1] and Jin Mao [1]

[1] Department of Mechanical Engineering, Xi'an University of Technology, No. 5 Jinhua South Road, Xi'an 710048, China; mouren.li931109@gmail.com (L.L.); 13488159576@163.com (Y.W.); tongzhao@xaut.edu.cn (T.Z.); maojin@xaut.edu.cn (J.M.)
[2] Zhejiang Zomax Transmission Co., Ltd., Wenling 317513, China
* Correspondence: 105266@xaut.edu.cn

Abstract

To address the insufficient fusion of electromechanical impedance (EMI) response features from multiple sensors and the limited characterization of spatial relationships between sensors and bolt nodes in four-bolt connection structures, this study proposes an improved graph convolutional network (GCN) model integrating Batch Normalization (BN) and Distance Weighting (DW) strategies for bolt preload-loss state identification. First, PZT sensor nodes and bolt nodes are jointly represented as a graph structure, and the correlation coefficient deviation (CCD) is extracted as the EMI response feature. Then, a weighted adjacency matrix is constructed according to the geometric distances between sensor nodes and bolt nodes to describe the spatial coupling relationships among different nodes. Subsequently, the weighted adjacency matrix and node features are input into the GCN, and a BN layer is introduced after the graph convolutional layers to reduce the influence of multi-channel feature distribution variations on model training stability. Experimental results on a four-bolt connection structure show that the proposed GCN-BN-DW model outperforms the Basic GCN, GCN-BN, GCN-DW, and several benchmark models in terms of prediction accuracy and stability. Under the strict five-fold cross-validation protocol, the proposed model achieves a test MAE of 2.400 ± 0.100, RMSE of 3.302 ± 0.239, MASE of 0.300 ± 0.013, and R^2 of 0.821 ± 0.033. These results indicate that the proposed model can effectively integrate multi-sensor EMI features and sensor–bolt spatial relationships, providing a feasible graph-based modeling approach for bolt preload-loss state identification.

Keywords: bolt preload; electromechanical impedance; graph convolutional network; multi-sensor fusion; batch normalization; distance weighting

Check for updates

Academic Editor: Tamara Nestorović

Received: 10 June 2026
Revised: 15 July 2026
Accepted: 17 July 2026
Published: 21 July 2026

Copyright: © 2026 by the authors. Licensee MDPI, Basel, Switzerland. This article is an open access article distributed under the terms and conditions of the Creative Commons Attribution (CC BY) license.

1. Introduction

Bolted connections are widely used in aerospace, high-speed rail, and various types of large-scale mechanical equipment due to their high structural reliability and ease of disassembly and maintenance [1]. However, during long-term service, the connection structure is continuously subjected to factors such as vibration, impact, temperature fluctuations, and load variations, which may cause the bolt preload to diminish. This can lead to a reduction in contact interface stiffness, changes in load transfer paths, and local stress redistribution [2]. If these changes are not detected and identified in a timely manner, they may further lead to connection loosening, fatigue damage, or even structural failure [3].

Therefore, conducting effective monitoring of the preload state of bolted joints is a critical research area for ensuring structural safety during service.

Electromechanical impedance (EMI) [4] is a high-frequency, localized, non-destructive testing method based on piezoelectric sensors. By exciting a piezoelectric element and measuring its impedance or admittance response under high-frequency excitation, it indirectly reflects changes in the local mechanical impedance of the structure. When the state of a bolted joint changes, the contact stiffness at the joint interface and the local load also change, thereby causing alterations in the peak, peak position, and spectral shape of the EMI frequency-domain response [5]. Consequently, EMI technology exhibits high sensitivity to bolt loosening and changes in preload status and has been widely applied in research on the health monitoring of bolted structures [6–10].

However, in complex multi-bolt connection structures, a single sensor or a single statistical metric struggles to comprehensively characterize the complex connection state. Spatial coupling exists between different bolt joints; a change in the preload state of a single bolt may affect the EMI response of multiple other sensors through the connecting plate, contact interface, and adjacent bolts [11]. Furthermore, due to differences in installation locations and propagation paths, the response amplitudes, frequency-sensitive ranges, and characteristic distributions of different sensors may vary significantly [12]. Therefore, relying on EMI characteristics from a single measurement point or traditional statistical indicators makes it difficult to fully describe the spatial relationships between sensor nodes and bolt nodes in multi-bolt connection structures.

In recent years, data-driven methods have been gradually introduced into EMI signal analysis and structural condition monitoring. Methods such as backpropagation neural networks and convolutional neural networks extract nonlinear features from impedance responses for use in research on bolt loosening detection, damage classification, and condition prediction [13–17]. Related studies have shown [18,19] that neural network methods offer certain advantages in EMI feature modeling, as they can reduce the influence of human bias on recognition results during feature selection. However, for structures with multiple sensors and multiple bolted connections, traditional neural networks typically treat features from each channel as ordinary vectors or matrices, making it difficult to explicitly represent sensor nodes, bolt nodes, and their spatial relationships. When multiple connection nodes exist within a structure, ignoring spatial topological relationships can result in the model's inability to adequately characterize local state changes.

Graph neural networks (GNNs) [20] can characterize the node associations and topological structure features of non-Euclidean data, making them suitable for describing the inter-node relationships within a structure. Among these, graph convolutional networks (GCNs) [21] aggregate node information through an adjacency matrix, enabling both node features and topological relationships to be incorporated into model training. For multi-sensor EMI monitoring, modeling sensors and bolt positions as graph nodes allows the use of graph structures to describe the spatial relationships between different measurement points and connecting nodes. Zhou [22] et al. combined EMI signals with GCNs to construct a sensor–bolt graph structure, achieving quantitative characterization of dual-bolt loosening states and validating the feasibility of integrating GCNs with EMI.

However, existing GCN and EMI modeling methods still have certain limitations. Current research primarily focuses on simplified two-bolt scenarios and has limited ability to characterize multi-node, multi-path coupling relationships in complex connection structures. In particular, for four-bolt connection structures, the increased number of bolts leads to complex coupling relationships between sensors, placing high demands on the model's ability to represent spatial relationships and ensure training stability. Existing EMI-GCN network frameworks do not adequately address the issues of multi-channel

feature distribution variations and training fluctuations, limiting the effectiveness of these frameworks in complex connection structures.

To address these issues, this paper proposes an improved GCN modeling method that integrates Distance Weighting (DW) [23] and Batch Normalization (BN) [24] strategies for the identification of preload-loss states in four-bolt connection structures. Different from previous EMI-GCN studies mainly focusing on simplified two-bolt monitoring cases, this work extends the sensor–bolt graph modeling framework to a four-bolt connection structure with 625 torque combinations. First, PZT sensor nodes and bolt nodes are jointly organized into a graph structure, and the CCD features extracted from multi-band EMI responses are used to characterize the variation in sensor responses relative to the reference state. Second, a weighted adjacency matrix is constructed based on the geometric distances between sensor nodes and bolt nodes to characterize the spatial relationships among nodes. Finally, node features and the weighted adjacency matrix are input into the GCN, and BN is introduced during the graph convolution feature propagation process to mitigate the impact of variations in multi-channel EMI feature distributions on the model training process. The contribution of this work is not the isolated use of GCN, DW, or BN alone, but the combined GCN-BN-DW framework for four-bolt preload-loss state identification using multi-sensor EMI features.Through experiments on four-bolt connection structures, a comparative analysis of the baseline GCN, GCN-BN, GCN-DW, and GCN-BN-DW models is conducted to validate the feasibility of the proposed method for bolt preload-loss state identification under the experimental conditions described in this paper.

2. Methods

2.1. Structural Modeling of Multi-Sensor EMI Maps

2.1.1. Extraction of EMI Signals and CCD Features

Electromechanical impedance (EMI) testing technology [25] is a non-destructive testing method based on the electromechanical coupling effect of piezoelectric materials. Figure 1 shows a schematic diagram of a one-dimensional electromechanical impedance theoretical model, in which a PZT piezoelectric ceramic patch is fixed at one end, and the host system can be modeled as a single-degree-of-freedom mass–spring–damping system. K, C, and V denote the equivalent structural stiffness, equivalent damping, and applied excitation voltage of the PZT patch, respectively. When the PZT is attached to the structural surface and subjected to a high-frequency excitation voltage, its impedance or admittance response is influenced by the local mechanical impedance of the structure. For bolted structures, changes in the preload state of the bolts alter the contact conditions and local stiffness at the joint interface, thereby causing changes in the peak values and waveform of the EMI frequency-domain response. Therefore, the EMI response can be used to characterize changes in the preload state of bolted structures.

To quantitatively characterize the degree of variation in EMI response relative to a reference state under different bolt preload states, this paper employs the correlation coefficient deviation (CCD) [26] as a sensor node feature. CC denotes the correlation coefficient between the EMI response under the current preload state and that under the reference state within the selected frequency range. Let $\mathrm{Re}(Z_1(i))$ denote the real part of the impedance response at frequency point i under the condition to be identified, and $\mathrm{Re}(Z_0(i))$ denote the real part of the impedance response at frequency point i under the initial condition; then, the correlation coefficient of the EMI response between the two conditions is expressed as:

$$CC_{\omega_1,\omega_2} = \frac{1}{\omega_2 - \omega_1} \sum_{i=\omega_1}^{\omega_2} \frac{\left[\mathrm{Re}(Z_0(i)) - \overline{Z}_0\right]\left[\mathrm{Re}(Z_1(i)) - \overline{Z}_1\right]}{\sigma_{Z_0}\sigma_{Z_1}} \quad (1)$$

$$CCD_{\omega_1,\omega_2} = 1 - CC_{\omega_1,\omega_2} \tag{2}$$

Here, $\overline{Z}_0$ and $\overline{Z}_1$ denote the mean values of the two impedance signals within the frequency range from ω_1 to ω_2, respectively, while σ_{Z_0} and σ_{Z_1} represent their corresponding standard deviations. For each sensor under each working condition, a CCD feature value can be calculated and used as the node input feature for constructing the graph model. When the bolted joint group is under the initial condition, the calculated CC is 1 and the CCD is 0.

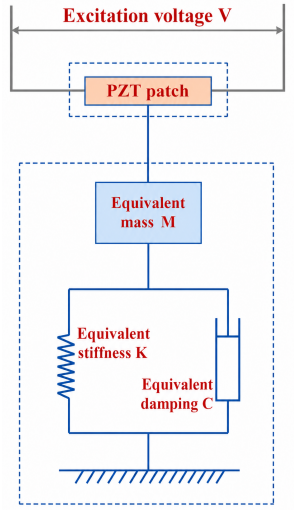


Figure 1. Schematic diagram of a one-dimensional electromechanical impedance (EMI) model.

2.1.2. Constructing the Sensor–Bolt Diagram Structure

The EMI response in a multi-bolt connection structure depends not only on the position of individual sensors but is also influenced by the spatial distance between the sensors and the bolt nodes, as well as the connection paths. To describe the spatial relationships among multiple nodes, this paper models both the PZT sensor nodes and the bolt nodes as a graph structure. Let there be N_s PZT sensor nodes and N_b bolt nodes, respectively, in the structure; then, the total number of nodes in the graph is:

$$N = N_s + N_b \tag{3}$$

Graph structures can be represented as:

$$G = (V, E, A, X) \tag{4}$$

Here, V is the set of nodes, comprising sensor nodes and bolt nodes; E is the set of edges, representing the spatial relationships between nodes; A is the adjacency matrix; and X is the node feature matrix.

The adjacency matrix $A = (a_{ij})$ represents the original topological connections between nodes, where a_{ij} is defined as:

$$a_{ij} = \begin{cases} 1, & \text{if nodes } v_i \text{ and } v_j \text{ are connected,} \\ 0, & \text{otherwise.} \end{cases} \tag{5}$$

The node feature matrix X represents the attribute information of each node, where the sensor node features consist of CCD values extracted from the corresponding channels, and the initial features of the bolt nodes are set to the zero vector. Through graph convolution modeling, the EMI characteristics of sensor nodes are propagated to bolt nodes via

adjacency relationships, thereby enabling the mapping and modeling of multi-sensor EMI characteristics to bolt preload-loss states.

For the four-bolt specimen in this study, the graph contains 14 nodes, including 10 PZT sensor nodes and 4 bolt nodes. Edges are established between PZT sensor nodes and bolt nodes to describe the sensor–bolt spatial coupling relationships. Direct sensor–sensor and bolt–bolt edges are not considered in the current graph construction. The initial features of the bolt nodes are set to zero, whereas the PZT sensor nodes contain the CCD feature vectors extracted from EMI responses.

2.1.3. Construction of the Distance-Weighted Adjacency Matrix

In multi-bolt connection structures, the EMI response measured by a PZT sensor is more sensitive to local impedance changes near the sensor. Therefore, the spatial distance between PZT sensor nodes and bolt nodes can be used as a measurable prior to describe the sensor–bolt coupling strength. For the present flat four-bolt plate specimen, a shorter sensor–bolt distance is assumed to indicate stronger local coupling, whereas a longer distance indicates weaker coupling [27]. Based on this consideration, a distance-weighted strategy is introduced into the adjacency matrix to describe the spatial relationship between sensor nodes and bolt nodes.

Let $P_i = (x_i, y_i, z_i)$ be the position vector of the ith node in the graph. The Euclidean distance between nodes i and j is calculated as:

$$d_{ij} = \left\| P_i - P_j \right\|_2 = \sqrt{(x_i - x_j)^2 + (y_i - y_j)^2 + (z_i - z_j)^2} \tag{6}$$

Based on the measured sensor–bolt distances, the distance-weighted adjacency matrix is constructed for the sensor–bolt graph. The measured distance d_{ij} is first normalized by the maximum measured sensor–bolt distance $d_{\max}$:

$$\bar{d}_{ij} = \frac{d_{ij}}{d_{\max}} \tag{7}$$

The distance-weighted adjacency matrix is then defined as:

$$A_{ij} = \begin{cases} \exp(-\beta_d \bar{d}_{ij}), & v_i \in V_s, v_j \in V_b \text{ or } v_i \in V_b, v_j \in V_s, \\ 0, & \text{otherwise} \end{cases} \tag{8}$$

where V_s and V_b denote the sets of PZT sensor nodes and bolt nodes, respectively; $\bar{d}_{ij}$ is the normalized sensor–bolt distance; and β_d is the distance attenuation coefficient.

The exponential Distance Weighting function assigns a larger edge weight to a closer sensor–bolt pair and a smaller edge weight to a farther pair. This function is continuous, monotonic, and bounded, and avoids the need for a manually selected distance threshold. The coefficient β_d controls the attenuation rate of the sensor–bolt coupling weight. In this study, β_d is set as a positive trainable parameter, so that the attenuation rate can be updated during model training.

It should be noted that the Euclidean distance is used as a first-order spatial prior rather than an exact EMI propagation path. The EMI response can also be affected by contact interfaces, load-transfer paths, boundary conditions, local stiffness variations, and sensor bonding conditions. Therefore, the distance-weighted graph in this study provides an approximate description of sensor–bolt spatial coupling for the present flat plate specimen. For more complex engineering structures, weights based on contact/load-transfer paths, experimentally identified sensitivity weights, or finite-element sensitivity-based weights may be needed.

To preserve the intrinsic characteristics of the nodes, self-loops are added to the adjacency matrix, as shown in Equation (9):

$$\widetilde{A} = A + I \tag{9}$$

Next, we compute the corresponding degree matrix $\widetilde{D}$, and all non-diagonal elements are zero, i.e., $\tilde{D}_{ij} = 0$ for $i \neq j$, whose diagonal elements satisfy:

$$\widetilde{D}_{ii} = \sum_{j=1}^{N} \widetilde{A}_{ij} \tag{10}$$

The adjacency matrix used for graph convolution propagation is then constructed using symmetric normalization:

$$\widehat{A} = \widetilde{D}^{-\frac{1}{2}} \widetilde{A} \widetilde{D}^{-\frac{1}{2}} \tag{11}$$

2.2. A GCN-Based Preload-Loss State Identification Model Integrating BN and DW

2.2.1. Basic GCN Feature Propagation

GCN aggregates information about the neighborhoods of nodes using an adjacency matrix and updates node features by incorporating trainable weights. For the lth layer of graph convolution, the propagation process is represented as follows:

$$H^{(l+1)} = \sigma\left(\hat{A} H^{(l)} W^{(l)}\right) \tag{12}$$

where $H^{(l)}$ represents the feature matrix of the lth layer, N is the number of nodes, and F is the feature dimension of the current layer; $W^{(l)}$ represents the trainable weight matrix of the lth layer; $\sigma(\cdot)$ is the nonlinear activation function. In this paper, the ReLU function is used; $H^{(0)} = X$ refers to the input feature matrix.

2.2.2. Batch Normalization

Both the sensor installation location and the response propagation path influence EMI characteristics, leading to variations in feature distribution across different channels. If these features are directly used as GCN inputs, the model may experience issues such as gradient oscillations, oscillatory propagation, or even convergence difficulties during training [28]. To mitigate this problem, this paper introduces Batch Normalization (BN) into the graph convolutional feature propagation process to normalize the output features of each graph convolutional layer [29].

The formula for Batch Normalization during training is as follows:

$$\mu_B = \frac{1}{m} \sum_{i=1}^{m} x_i \tag{13}$$

$$\sigma_B^2 = \frac{1}{m} \sum_{i=1}^{m} (x_i - \mu_B)^2 \tag{14}$$

$$\hat{x}_i = \frac{x_i - \mu_B}{\sqrt{\sigma_B^2 + \varepsilon}} \tag{15}$$

$$\hat{y}_i = \gamma \hat{x}_i + \beta_{BN} \tag{16}$$

Here, m represents the number of samples in the current batch, $\hat{x}_i$ denotes the input feature of the i-th sample in the mini-batch, μ_B and σ_B^2 are the batch mean and batch variance, respectively; ε is a small constant used to avoid division by zero; and γ and β_{BN} are trainable scale and shift parameters. The notation β_{BN} is used to distinguish the

BN shift parameter from the distance attenuation coefficient β_d in the distance-weighted adjacency matrix. During inference, the running mean and running variance accumulated during training are used for normalization.

2.2.3. Model Output and Loss Function

In this paper, bolt nodes are treated as the nodes to be predicted. By aggregating the EMI features from sensor nodes via a multi-layer GCN, the model performs regression prediction of the target torque level of each bolt node. Let y_b denote the true label for b bolt nodes, and $\hat{y}_b$ denote the model's predicted value. For a single sample, the model output is expressed as:

$$\hat{Y} = [\hat{y}_1, \hat{y}_2, \ldots, \hat{y}_{N_b}] \tag{17}$$

Here, $\hat{Y}$ represents the predicted results for all bolted joints. The model training process uses the mean squared error as the loss function:

$$\mathcal{L}_{MSE} = \frac{1}{N_b} \sum_{b=1}^{N_b} (y_b - \hat{y}_b)^2 \tag{18}$$

For batch training samples, the loss function is averaged across the sample dimension. By minimizing the error between the predicted values and the true labels, the model learns the mapping relationship between multi-sensor EMI features, spatial relationships among nodes, and bolt preload-loss states. The overall workflow of the GCN-BN-DW model proposed in this paper is shown in Figure 2, which includes EMI feature extraction, distance-weighted matrix construction, graph convolutional feature propagation, Batch Normalization, and bolt node state regression prediction.

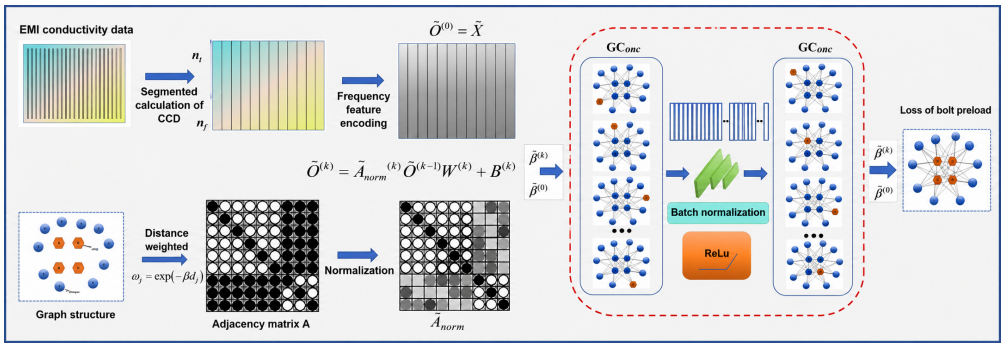


Figure 2. Recognition framework diagram of the improved GCN model.

3. Experimental Design and Conductance Response Analysis

In this section, an experimental system consisting of an aluminum alloy plate with four-bolt connections was constructed to collect multi-sensor EMI response data under different preload-loss states, with the aim of verifying the feasibility of the multi-sensor EMI-based graph modeling method. The experimental content includes system setup, specimen design, configuration of torque-defined preload-loss states, measurement of spatial distances between sensors, and analysis of EMI response patterns. By comparing conductance curves under different sensor positions and preload-loss states, this study analyzes the sensitivity of multi-sensor EMI responses to changes in bolt connection states, providing experimental data for subsequent CCD feature extraction and graph structure modeling.

3.1. Experimental Equipment and Test Specimens

3.1.1. Experimental Equipment

The experimental system consists of a desktop computer, a precision impedance analyzer, PZT sensors, and a four-bolt-connected aluminum alloy plate test specimen,

as shown in Figure 3. The impedance analyzer is the IM3536 model from Hioki (Japan), which features high precision and wide-frequency response capabilities; its main technical parameters are detailed in Table 1. The PZT sensor has a diameter of 15 mm and a thickness of 1 mm, with the material type designated as PZT-5. The bolt preload is adjusted via torque control using a BS04-135BN torque wrench, which has a measurement range of 6.8 N·m to 135 N·m and a torque measurement accuracy of ±3%.

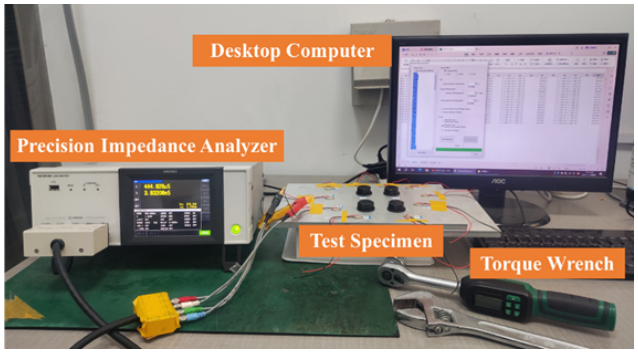


Figure 3. Multi-bolt experimental monitoring system.

Table 1. Specifications of the IM3536 precision impedance analyzer.

Parameters	Indicators
Rated voltage	240 V
Measurement range	4 Hz–8 MHz
Measurement accuracy	±0.05%rdg
Minimum measurement increment	0.1 Hz
Maximum voltage/current excitation frequency	8 MHz
Fastest measurement time	1 ms

3.1.2. Test Specimen Model

To verify the effectiveness of the aforementioned graph convolutional modeling method in the fusion of multi-sensor EMI responses, the test specimen was designed as an aluminum alloy plate structure connected by four bolts; the 3D model is shown in Figure 4. The test specimen measures 300 mm × 200 mm × 10 mm and is rigidly connected using four M16 Grade 12.9 chromium–molybdenum alloy steel bolts. The four bolt joints are designated as B1, B2, B3, and B4, respectively.

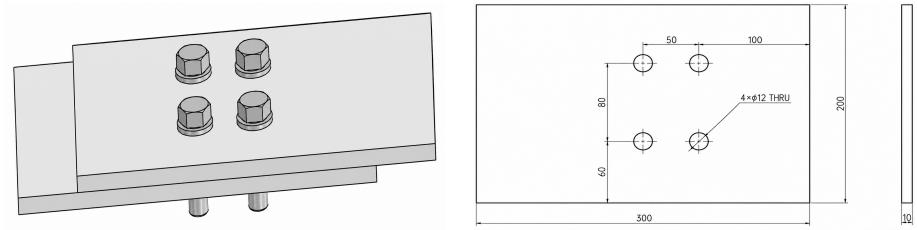


Figure 4. Geometry and dimensions of the four-bolt aluminum alloy specimen.

3.2. Experimental Setup

Based on the piezoelectric coupling characteristics of piezoelectric materials, a self-excited piezoelectric admittance monitoring system was constructed. In the experiment, 10 PZT sensors were secured to different positions on the surface of an aluminum alloy plate using epoxy resin, and wires were soldered to the positive and negative terminals of the sensors. The aluminum alloy plate with the four-bolt connection after the sensors were attached is shown in Figure 5. The PZT sensors were not arranged in a circularly symmetric

pattern because the monitored specimen was a rectangular four-bolt joint rather than an axisymmetric structure. The purpose of the sensor layout was to cover different regions around the bolt group and to provide diverse sensor–bolt distances for subsequent distance-weighted graph modeling. In addition, practical constraints, including bolt positions, wiring space, edge distance of the plate, and available bonding areas, were considered during sensor installation. Therefore, the adopted PZT layout was designed to balance spatial coverage, installation feasibility, and sensitivity to different bolt preload-loss states.

During the experiment, an impedance analyzer applied a swept voltage excitation signal to the PZT sensors. The sweep frequency range was set from 10 Hz to 1 MHz, with an excitation amplitude of 1 V, and the conductance response of each sensor was collected. The selected frequency range was not determined solely based on the global natural frequencies of the aluminum plate–bolt assembly. In contrast to conventional modal testing, EMI measurements mainly reflect the local electromechanical interaction between the PZT patch and the host structure. Therefore, a broadband frequency sweep was adopted to cover the effective response range of the PZT sensors and to identify conductance peaks and preload-sensitive frequency bands for subsequent feature extraction.

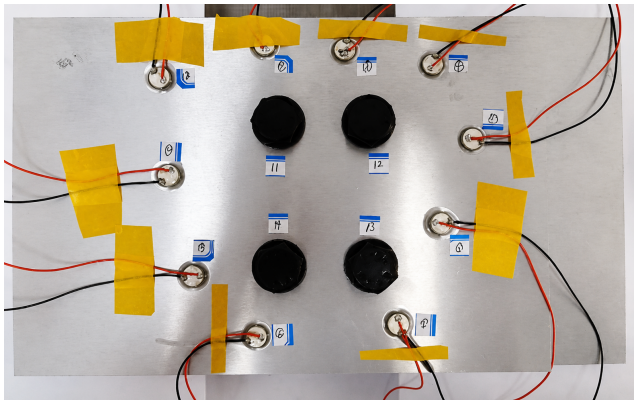


Figure 5. Aluminum alloy panel with PZT bonded in place using a four-bolt connection.

This study focuses on the identification of torque-defined preload-loss states in multi-bolt connections. In the experiment, 30 N·m was defined as the reference tightened state. To simulate different degrees of bolt loosening, the applied torque of each bolt was gradually reduced from 30 N·m to 10 N·m with a step size of 5 N·m. Therefore, five target torque levels were considered for each bolt: 30, 25, 20, 15, and 10 N·m, where a lower torque level was used to represent a larger preload reduction relative to the reference tightened state. The target torque levels for a single bolt are shown in Table 2.

Table 2. Target torque levels for a single bolt.

Torque-Defined State	Target Torque Level
Reference state	30 N·m
State 1	25 N·m
State 2	20 N·m
State 3	15 N·m
State 4	10 N·m

It should be noted that the applied torque levels were used as controlled indicators of preload-loss states rather than direct measurements of bolt axial preload. The relationship between the applied torque and the axial preload can be approximately expressed as $T = KFd$, where T is the applied torque, F is the axial preload, d is the nominal bolt diameter, and K is the torque coefficient related to friction and contact conditions. Since K

is affected by thread friction, bearing surface friction, and contact uncertainty, the labels in this work should be interpreted as torque-defined preload-loss states under the present experimental conditions.

For the four-bolt connection, each bolt could be assigned one of the five target torque levels, namely 10, 15, 20, 25, and 30 N · m. Consequently, a total of $5^4 = 625$ torque combinations were generated. Each operating condition represents a specific target torque combination of bolts B1, B2, B3, and B4, rather than the chronological order of tightening or loosening. For example, condition 30303030 indicates that all four bolts were in the reference tightened state of 30 N · m, whereas condition 10152025 indicates that bolts B1, B2, B3, and B4 were set to 10, 15, 20, and 25 N · m, respectively.

During the experiment, all four bolts were first tightened to 30 N · m to acquire the reference EMI response under the initial tightened state. Then, according to the predefined test plan, the target torque of each bolt was adjusted to the prescribed value in the corresponding torque combination using a calibrated digital torque wrench. After each target torque combination was reached, the specimen was kept undisturbed for 5 min to reduce the influence of short-term relaxation and manual loading disturbances. Subsequently, the conductance responses of the 10 PZT sensors were collected using the impedance analyzer. After all 625 torque combinations were tested, all bolts were fully unloaded. After a one-day interval, the same loading–resting–data acquisition procedure was repeated to evaluate the repeatability of the experimental protocol. The representative test conditions for the four-bolt torque combinations are listed in Table 3.

Table 3. Test conditions for torque combinations of four-bolt connections.

	Bolt 1	**Bolt 2**	**Bolt 3**	**Bolt 4**
Operating Condition 1	10 N·m	10 N·m	10 N·m	10 N·m
Operating Condition 2	10 N·m	10 N·m	10 N·m	15 N·m
...	...	...	...	...
Operating Condition 623	30 N·m	30 N·m	30 N·m	20 N·m
Operating Condition 624	30 N·m	30 N·m	30 N·m	25 N·m
Operating Condition 625	30 N·m	30 N·m	30 N·m	30 N·m

In multi-sensor EMI monitoring, the spatial relationship between sensors and bolts affects the intensity of the EMI response to local state changes. To construct a distance-weighted adjacency matrix, the geometric distances between each PZT sensor node and the four bolt nodes were measured in the experiment; the results are shown in Table 4. This distance matrix is used to calculate edge weights in graph-based modeling to characterize the spatial relationships between sensor nodes and bolt nodes.

Table 4. Distance parameters between sensor nodes and bolt nodes for four-bolt connection monitoring.

	Bolt 1	**Bolt 2**	**Bolt 3**	**Bolt 4**
Sensor 1	71.01 mm	116.56 mm	154.95 mm	120.94 mm
Sensor 2	43.81 mm	72.56 mm	133.34 mm	124.82 mm
Sensor 3	56.85 mm	41.92 mm	117.31 mm	127.08 mm
Sensor 4	94.55 mm	47.65 mm	115.48 mm	144.12 mm
Sensor 5	106.25 mm	59.61 mm	89.15 mm	127.68 mm
Sensor 6	104.22 mm	69.95 mm	45.92 mm	94.48 mm
Sensor 7	128.75 mm	113.93 mm	35.51 mm	71.07 mm
Sensor 8	117.16 mm	130.65 mm	72.62 mm	39.65 mm
Sensor 9	96.39 mm	127.46 mm	96.79 mm	46.91 mm
Sensor 10	65.54 mm	112.56 mm	119.62 mm	78.01 mm

Figure 6 shows a schematic diagram illustrating the spatial relationships among four bolt nodes (B1, B2, B3, and B4) and three PZT sensor nodes. The lines in the figure are used solely to illustrate the concept of Distance Weighting; in actual modeling, a graph structure is constructed using all sensor nodes and bolt nodes, and adjacency relationships are established based on the distances between nodes.

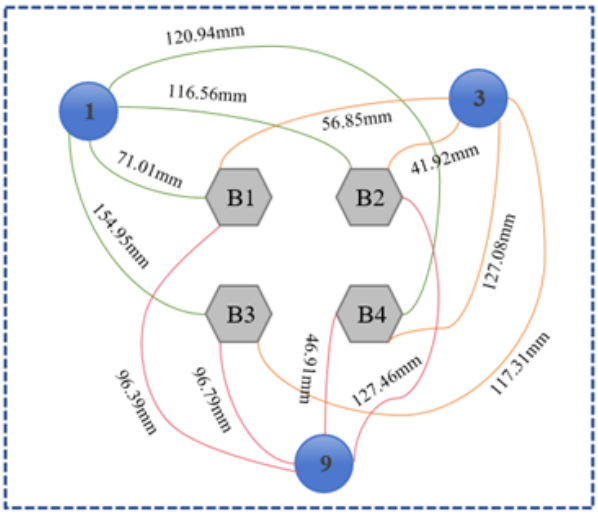


Figure 6. Schematic diagram of distance weighting.

3.3. Analysis of Conductance Response Results

To analyze the patterns of changes in bolt preload caused by multi-sensor EMI signals, a comparative analysis was conducted on the conductance curves collected by different PZT sensors. Figure 7 shows the conductance response curves of 10 PZT sensors under operating condition 30303030.

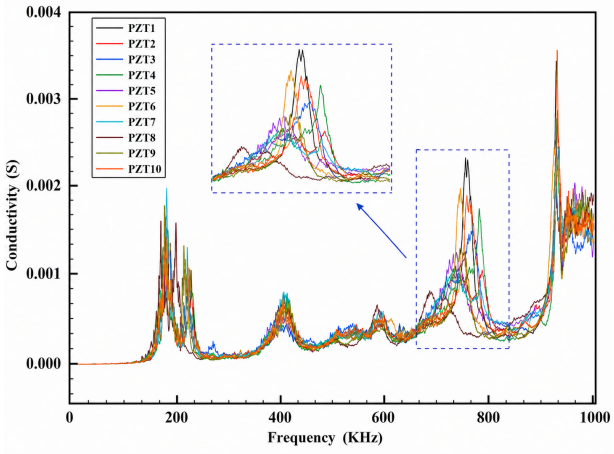
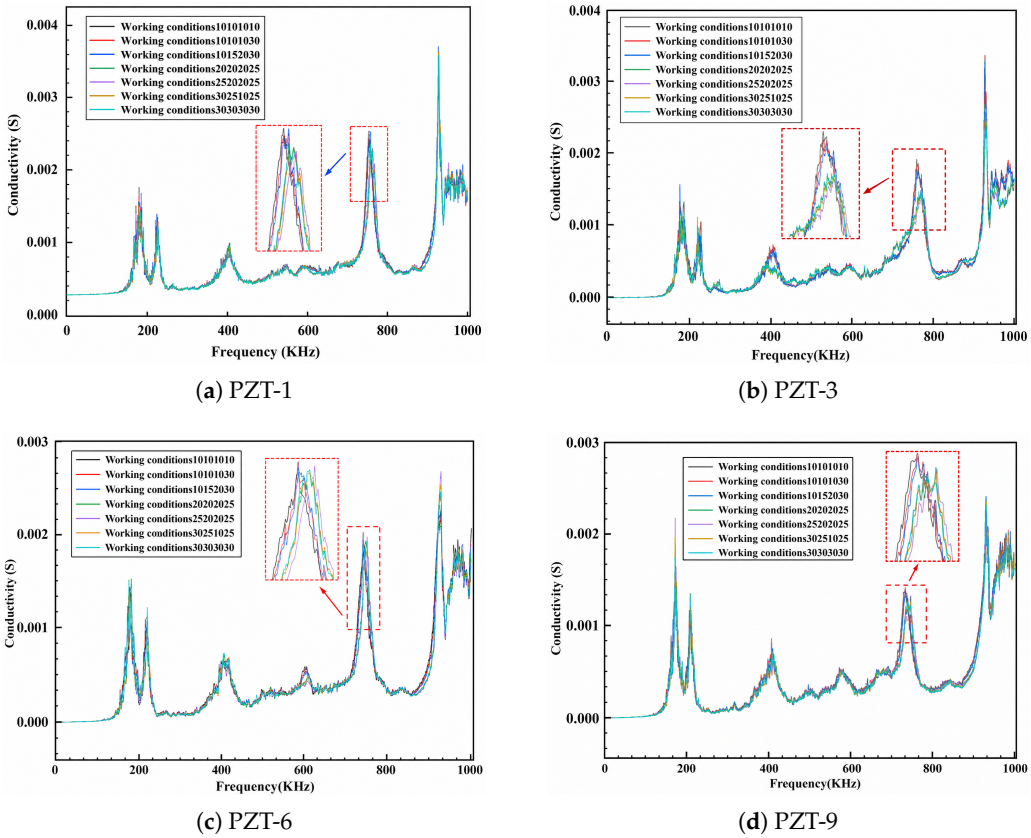


Figure 7. Conductance response of PZT sensors at different locations under operating condition 30303030.

As shown in Figure 7, the conductance curves measured by PZT sensors at different locations exhibit essentially consistent peak positions at the main resonance frequency, but differ in terms of local peak amplitude, peak shape, and fine-scale variations. This indicates that the PZT response is not only related to the overall structural state but also to the sensor installation location and the propagation path between bolted joints. For multi-bolt connection structures, relying on a single PZT sensor alone makes it difficult to comprehensively characterize changes in the preload state of different bolt joints; therefore, it is necessary to adopt a multi-sensor information fusion modeling method.

To further analyze the response changes of the same sensor under different preload state, Figure 8 plots the conductance curves of PZT-1, PZT-3, PZT-6, and PZT-9 under different operating conditions.



(**a**) PZT-1 (**b**) PZT-3

(**c**) PZT-6 (**d**) PZT-9

Figure 8. Conductance curves under different operating conditions in a test to monitor the preload state of multi-bolt connections. (**a**) PZT-1; (**b**) PZT-3; (**c**) PZT-6; (**d**) PZT-9.

As shown in Figure 8, as the bolt assembly state changes, the peak amplitude, peak position, and peak shape of the conductance curve vary across certain frequency bands, indicating that the EMI signal is sensitive to changes in the connection state. Under identical operating conditions, different position sensors exhibit varying response intensities and sensitive frequency bands, indicating that each sensor reflects structural state information from different local regions and propagation paths. The response changes of the same sensor under different bolt combination conditions do not follow a linear relationship, suggesting that changes in the preload state of multiple bolts have a coupled effect on local admittance characteristics.

4. Analysis of Modeling and Recognition Results Using a Graph Neural Network That Integrates BN and DW

Building upon the experimental data and graph structures presented in Section 3, this chapter constructs an improved graph convolutional network (GCN) model that integrates Batch Normalization (BN) and Distance Weighting (DW) strategies to perform regression prediction of the preload-loss state of a four-bolt connection structure using multi-sensor EMI features.By comparing the proposed model with Basic GCN, GCN-BN, GCN-DW, and several benchmark models, the roles of BN and DW strategies in multi-sensor EMI graph modeling are analyzed, and the predictive performance of the proposed model is evaluated under the experimental conditions described in this paper.

4.1. Multi-Sensor Feature Extraction and Fusion

To establish a mapping model between multi-sensor EMI response features and bolt preload state, this paper constructs a graph neural network model based on the basic GCN framework that integrates spatial relationships between nodes and multi-channel feature information. The nodes in the graph consist of both PZT sensor nodes and bolt nodes. The sensor nodes are used to input CCD features calculated from EMI responses, while the bolt nodes serve as the nodes to be predicted, outputting the predicted target torque levels for the corresponding bolts.

The model employs a multi-layer graph convolutional network for feature propagation among nodes. The EMI features from sensor nodes are aggregated within the graph structure via an adjacency matrix and transmitted to bolt nodes. The adjacency matrix A is an n×n matrix, where n represents the total number of nodes in the graph. Based on the geometric distances between sensor nodes and bolt nodes measured in Section 3, this paper constructs a distance-weighted adjacency matrix to characterize the spatial relationships between nodes.

In traditional GCNs, the adjacency matrix merely reflects node connectivity, making it difficult to distinguish the impact of spatial distance differences between nodes on the propagation of EMI responses. For multi-bolt connection structures, the distance between sensor nodes and bolt nodes affects the sensitivity of sensors to changes in local preload state. Therefore, this paper introduces DW during the construction of the adjacency matrix and uses an exponential decay function to define node edge weights:

$$\omega_{ij} = \exp(-\beta d_{ij}) \tag{19}$$

Here, d_{ij} represents the geometric distance between the i-th node and the j-th node, and β is the distance decay coefficient. This definition assigns greater weights to nodes that are closer together and reduces the weights of nodes that are farther apart, thereby enabling the graph structure to reasonably reflect the spatial relationships between sensor nodes and bolt nodes.

Additionally, due to variations in PZT installation positions and response propagation paths, the EMI characteristics of each channel differ in both amplitude and distribution. To mitigate the impact of these variations on the stability of model training, this paper introduces Batch Normalization (BN) during the graph convolution feature propagation process to normalize the node features after each layer of graph convolution. BN adjusts the distribution of propagated features to reduce the impact of inconsistent feature scales across different channels on the training process.

Figure 9 illustrates the construction of the adjacency matrix for a four-bolt connection structure. First, node distances are calculated based on the spatial positions of the sensor nodes and bolt nodes. Then, a weighted adjacency matrix is constructed using distance-weighted values, which is further utilized as the adjacency matrix for GCN feature propagation.

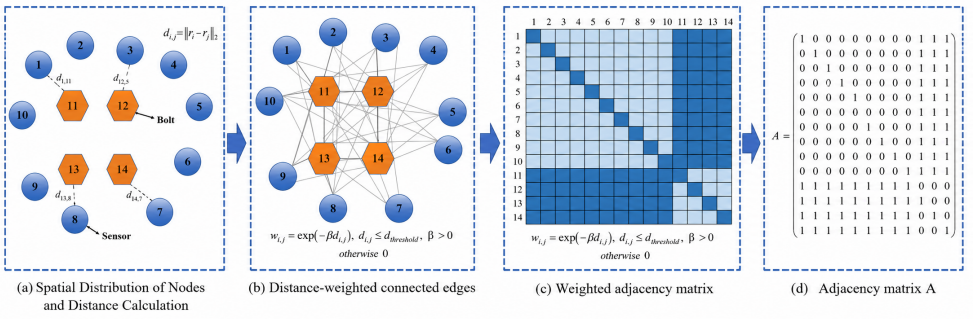


Figure 9. Schematic diagram of the adjacency matrix for a four-bolt connection structure.

4.2. Model Performance Evaluation and Results Analysis

4.2.1. Hyperparameter Settings

To ensure the comparability of prediction results across different models, this paper adopts uniform training parameter settings for model performance evaluation and ablation experiments. Except for the BN and DW modules, all models are consistent in terms of input features, number of network layers, hidden layer dimensions, optimizer, learning rate, and loss function, in order to minimize the impact of training parameter differences on model performance comparisons.

During model training, Mean Squared Error (MSE) was used as the loss function to minimize the deviation between the predicted and actual target torque levels; Adam was used as the optimizer for parameter updates. The learning rate was set to 0.001, the batch size to 64, the L2 regularization coefficient to 5×10^{-4}, and the dropout retention rate to 0.8. The GCN model employed three layers of graph convolutional hidden layers with the ReLU activation function; the specific parameter settings are shown in Table 5.

Table 5. Model parameter settings.

Name	Value
Number of hidden layers in the convolutional layer	3
Batch size	64
Learning rate	0.001
Activation function	ReLU
Loss function	Mean Squared Error Loss
Optimizer	Adam
L2 regularization coefficient	5×10^{-4}
Dropout retention rate	0.8

To evaluate the generalization ability of the proposed model, a strict five-fold cross-validation strategy was adopted. In each fold, one subset was held out as the test set and was used only for final performance evaluation. The remaining samples were further divided into training and validation subsets, where the validation subset was used for early stopping and model selection. To avoid information leakage, the normalization parameters were calculated only from the training subset and then applied to the validation and test subsets. All evaluation results were reported as the mean $\pm$ standard deviation over the five folds.

4.2.2. Evaluation Metrics

To quantitatively evaluate the performance of different graph convolutional neural network (GCN) models in the four-bolt preload prediction task, the Mean Absolute Error (MAE), Root Mean Square Error (RMSE), Mean Absolute Scaled Error (MASE), and Coefficient of Determination (R^2) are selected as evaluation metrics.

MAE is used to characterize the average absolute deviation between the predicted results and the true values; a lower value indicates that the predicted values are closer to the true values. RMSE is calculated by taking the square root of the sum of the squares of the errors and then taking the square root, reflecting the dispersion of the predicted results. MASE is used as a dimensionless supplementary metric by scaling the mean absolute prediction error with the mean absolute variation between adjacent reference preload states. R^2 is used to measure the model's ability to explain the overall variation in the data; a value closer to 1 indicates better model fitting performance. The formulas for each evaluation metric are as follows:

$$\mathrm{MAE} = \frac{1}{n}\sum_{i=1}^{n}|y_i - \hat{y}_i| \tag{20}$$

$$R^2 = 1 - \frac{\sum_{i=1}^{n}(y_i - \hat{y}_i)^2}{\sum_{i=1}^{n}(y_i - \bar{y})^2} \tag{21}$$

$$\mathrm{RMSE} = \sqrt{\frac{1}{n}\sum_{i=1}^{n}(y_i - \hat{y}_i)^2} \tag{22}$$

$$\mathrm{MASE} = \frac{\frac{1}{n}\sum_{i=1}^{n}|y_i - \hat{y}_i|}{\frac{1}{n-1}\sum_{i=2}^{n}|y_i - y_{i-1}|} \tag{23}$$

In the equation, y_i represents true target torque level of the i-th sample, $\hat{y}_i$ represents the predicted target torque level, $\bar{y}$ represents the mean value of the true target torque levels, and n represents the number of samples. For MAE, RMSE, and MASE, a smaller value indicates a lower prediction error; for R^2, a value closer to 1 indicates that the model better fits the variations in the true data.

Figure 10 shows the training and validation loss curves of the GCN-BN-DW model. The training loss decreases continuously with the increase of epochs, indicating that the model gradually learns the mapping relationship between multi-sensor EMI features and bolt preload-loss states. The validation loss also decreases rapidly in the early training stage and then tends to stabilize. Although a gap between the training and validation losses can be observed, the validation loss does not exhibit a continuous increasing trend, indicating that the training process is stable and no severe overfitting occurs under the current validation setting.

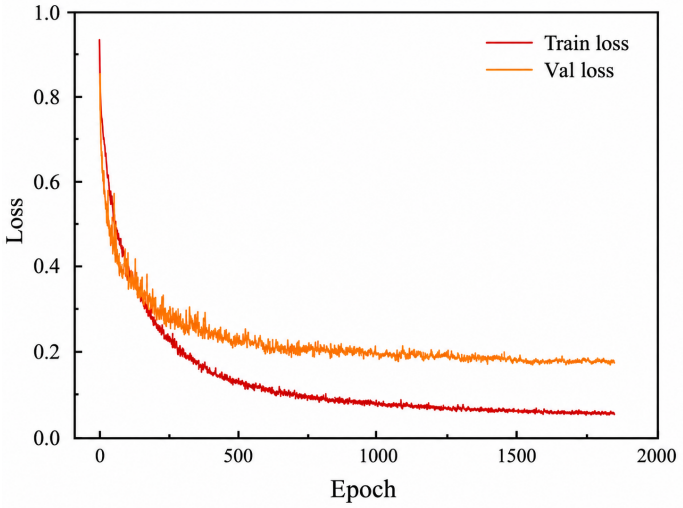


Figure 10. Training and validation loss curves of the GCN-BN-DW model.

4.2.3. Comparison of Model Prediction Results and Performance

To ensure a fair comparison, all benchmark models were evaluated using the same five-fold cross-validation protocol. In each fold, the test subset was held out for final evaluation only, and the remaining samples were further divided into training and validation subsets. To avoid information leakage, the normalization parameters of input features and labels were calculated only from the training subset and then applied to the validation and test subsets.

For non-graph benchmark models, the CCD features from 10 PZT sensors and 12 sub-bands were reshaped into a 120-dimensional feature vector. For graph-based models, the input graph contained 14 nodes, including 4 bolt nodes and 10 PZT sensor nodes.

Each sensor node used a 12-dimensional CCD feature vector, while the bolt nodes were initialized with zero feature vectors. The main implementation settings of the benchmark models are summarized in Table 6.

Table 6. Implementation settings of benchmark models.

Model	Input Representation	Main Implementation Settings
SVR	120-dimensional CCD feature vector	Multi-output SVR with RBF kernel; $C = 1.0$, $\epsilon = 0.1$, $\gamma =$ scale
RF	120-dimensional CCD feature vector	Random forest regressor; 200 trees; max depth = None
MLP	120-dimensional CCD feature vector	Fully connected network with hidden dimensions 128–64–32; BN, ReLU
CNN	10×12 CCD feature map	Two convolutional blocks followed by fully connected layers
GAT	14-node graph with 12-dimensional node features	Two graph attention layers; hidden dimension = 64; attention heads = 4
GCN-BN-DW	14-node graph with 12-dimensional node features	Three GCN layers with hidden dimensions 128–64–32; distance-weighted adjacency and BN

The SVR and RF models were used as conventional machine-learning baselines. The MLP and CNN models were used as non-graph deep learning baselines. The GAT model was used as a graph neural network baseline with attention-based aggregation. Compared with these models, the proposed GCN-BN-DW model further introduces the distance-weighted adjacency matrix and BN in graph feature propagation.

To verify the feasibility of the multi-sensor EMI mapping method for predicting the preload-loss state of four-bolt connections, the proposed GCN-BN-DW model was evaluated under the strict five-fold cross-validation protocol. The benchmark comparison results are shown in Figure 11. The quantitative results show that the proposed model can establish an effective mapping relationship between multi- sensor EMI features and bolt preload-loss states. The detailed prediction distributions of different GCN variants are further analyzed in the ablation study.

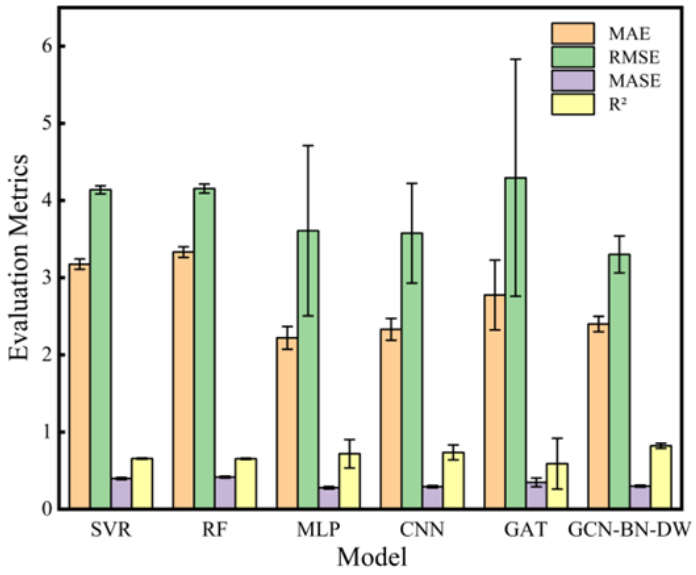


Figure 11. Benchmark comparison of different models.

The benchmark comparison further demonstrates that the proposed GCN-BN-DW model achieves superior prediction performance under the same validation protocol. These results indicate that graph-based fusion of multi-sensor EMI features is more suitable for bolt preload-loss identification than conventional machine-learning models and general deep-learning models. The detailed contribution of the BN and DW modules is further analyzed in the following ablation study.

4.2.4. Analysis of Ablation Experiment Results

To further investigate the effects of the BN and DW modules on model performance, an ablation study was conducted under the same five-fold cross-validation protocol. The Basic GCN model was used as the baseline. GCN-BN and GCN-DW were constructed by introducing only the BN module and the DW module, respectively, while the proposed GCN-BN-DW model integrates both modules. For all comparison models, the input features, dataset partitioning, training parameters, loss function, and evaluation metrics were kept consistent to ensure a fair comparison.

Table 7 summarizes the ablation results of different GCN variants under five-fold cross-validation. The Basic GCN model provides the baseline prediction performance, indicating that the graph structure can establish a preliminary mapping between multi-sensor EMI features and bolt preload-loss states. Compared with the Basic GCN model, introducing BN or DW individually changes the prediction performance to different extents. The BN module helps stabilize the propagated feature distribution during graph convolution, while the DW module improves the spatial representation of the graph by incorporating the distance-dependent relationship between PZT sensors and bolt nodes. When BN and DW are combined, the GCN-BN-DW model achieves the best overall performance, with lower MAE, RMSE, and MASE values and a higher R^2 value. This indicates that BN and DW play complementary roles in multi-sensor EMI feature fusion and graph-based preload-loss prediction.

Table 7. Ablation study of the BN and DW modules under five-fold cross-validation.

Model	MAE	RMSE	MASE	R^2
Basic GCN	2.568 ± 0.211	3.854 ± 0.832	0.321 ± 0.026	0.690 ± 0.146
GCN-BN	2.500 ± 0.153	3.756 ± 0.814	0.313 ± 0.017	0.706 ± 0.131
GCN-DW	2.733 ± 0.226	3.852 ± 0.619	0.342 ± 0.023	0.696 ± 0.105
GCN-BN-DW	2.400 ± 0.100	3.302 ± 0.239	0.300 ± 0.013	0.821 ± 0.033

To further examine whether the observed performance differences were affected by fold-to-fold variations, a statistical comparison was conducted based on the five-fold cross-validation results reported in Table 7. Since the comparison was performed using the summarized mean and standard deviation values, Welch's *t*-test was adopted as supplementary statistical evidence. As shown in Table 8, the GCN-BN-DW model shows better mean performance than the other GCN variants. Compared with GCN-DW, the improvements in MAE and MASE are statistically significant, with *p*-values lower than 0.05, while the improvement in R^2 is close to the 0.05 significance level. The comparisons with Basic GCN and GCN-BN show improved mean values but do not reach the 0.05 significance level. Therefore, the statistical results are used as supplementary evidence that the combined BN-DW strategy improves the prediction performance and stability of the graph model.

Table 8. Statistical comparison of GCN variants under five-fold cross-validation.

Comparison	MAE p-Value	RMSE p-Value	MASE p-Value	R^2 p-Value
GCN-BN-DW vs. Basic GCN	0.161	0.217	0.158	0.115
GCN-BN-DW vs. GCN-BN	0.261	0.288	0.214	0.122
GCN-BN-DW vs. GCN-DW	0.026	0.121	0.011	0.054

To further examine the role of BN in the GCN-BN-DW model, the feature distribution before and after BN was analyzed using the five-fold cross-validation results. The channel-wise standard deviation was calculated and normalized by the mean standard deviation of the corresponding stage.

As shown in Table 9 and Figure 12, the coefficient of variation of the channel-wise standard deviation decreases from 0.267 ± 0.032 before BN to 0.168 ± 0.051 after BN. This result indicates that BN reduces the relative scale difference among different feature channels after graph convolution. Therefore, DW introduces distance-dependent sensor–bolt relationships, while BN reduces the relative scale difference among propagated feature channels. This provides additional evidence for the combined use of BN and DW in the proposed model.

Table 9. Feature distribution statistics before and after BN.

Stage	Mean Channel Std	Std. of Channel Std	CV
Before BN	0.448 ± 0.075	0.121 ± 0.032	0.267 ± 0.032
After BN	1.013 ± 0.171	0.177 ± 0.078	0.168 ± 0.051

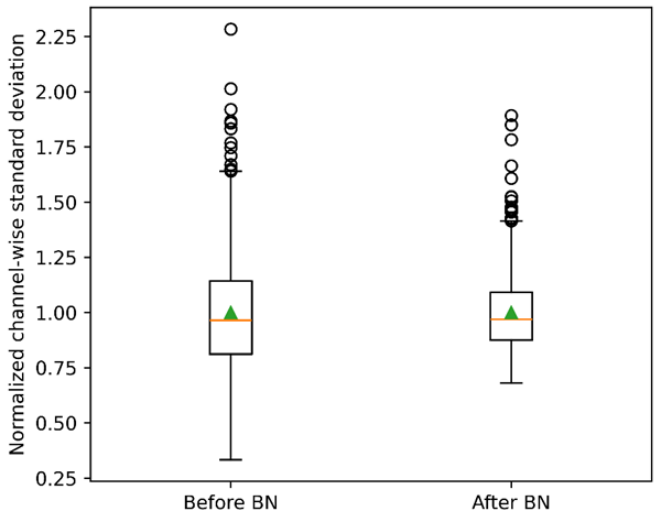
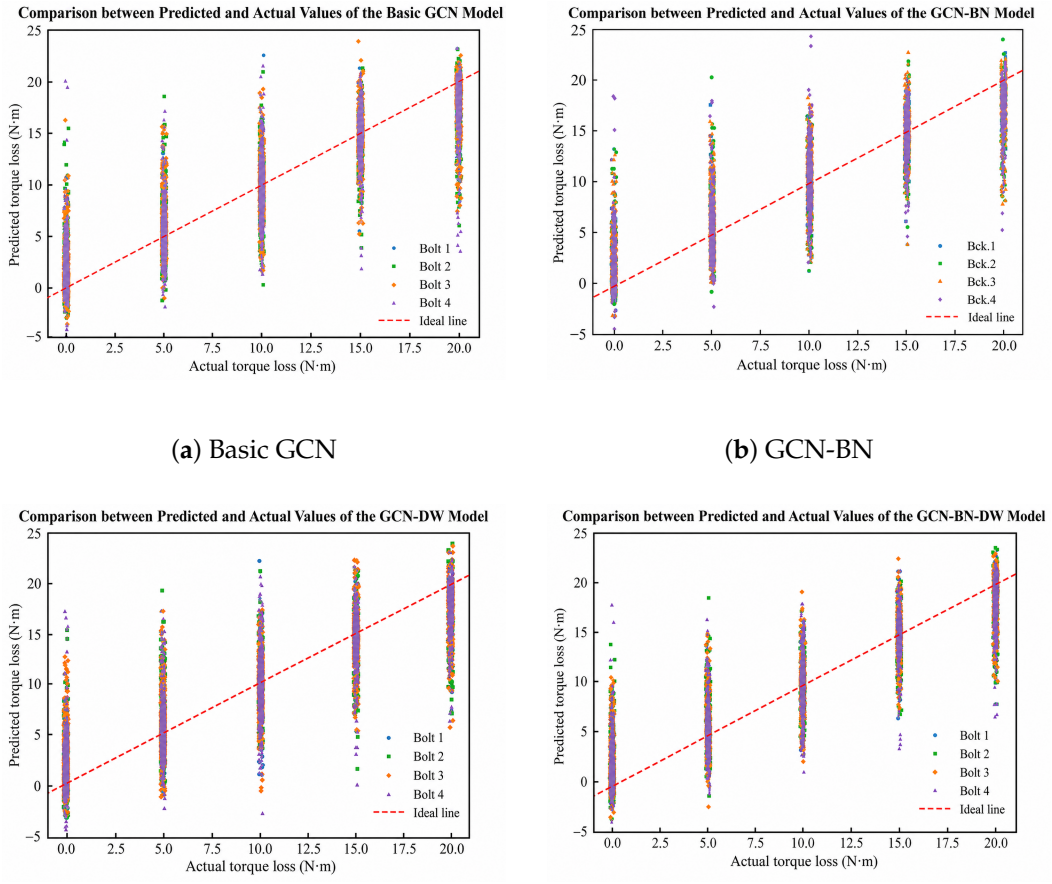


Figure 12. Normalized channel-wise standard deviations before and after BN in the GCN-BN-DW model.

To provide a more intuitive comparison of the prediction behavior of different GCN variants, the predicted-versus-actual distributions of Basic GCN, GCN-BN, GCN-DW, and GCN-BN-DW are shown in Figure 13. The scatter plots show that the prediction results of Basic GCN, GCN-BN, and GCN-DW still exhibit noticeable dispersion at different preload-loss levels. In contrast, the GCN-BN-DW model presents a more concentrated distribution around the ideal prediction line, indicating that the combined BN-DW strategy improves both the stability of feature propagation and the spatial representation capability of the graph model.



(**a**) Basic GCN (**b**) GCN-BN

(**c**) GCN-DW (**d**) GCN-BN-DW

Figure 13. Prediction distributions of different GCN variants under five-fold cross-validation: (**a**) Basic GCN; (**b**) GCN-BN; (**c**) GCN-DW; (**d**) GCN-BN-DW.

5. Conclusions

This paper addresses the issues of fusing multi-sensor EMI response characteristics and identifying torque-defined preload-loss states in multi-bolt connection structures by proposing an improved graph convolutional network (GCN) model that integrates Batch Normalization (BN) and Distance Weighting (DW) strategies. This method constructs a graph structure that integrates sensor nodes and bolt nodes. It uses the coefficient of correlation deviation (CCD) to characterize the degree of variation in sensor EMI responses relative to the reference state and constructs a distance-weighted adjacency matrix based on the geometric distances between sensor nodes and bolt nodes. On this basis, GCN is used to propagate and fuse features from multiple sensor nodes to the bolt node, and BN is introduced during the graph convolutional feature propagation process to mitigate the impact of multi-channel EMI feature distribution variations on model training stability.

Experimental results indicate that, under the strict five-fold cross-validation protocol, the proposed GCN-BN-DW model achieves better prediction performance than the Basic GCN, GCN-BN, and GCN-DW models. The proposed model obtains lower MAE, RMSE, and MASE values and a higher R^2 value, indicating that the integration of BN and DW improves both prediction accuracy and model stability. Compared with conventional machine-learning models and general deep-learning models, the GCN-BN-DW model also shows better overall performance, demonstrating the effectiveness of graph-based multi-sensor EMI feature fusion for bolt preload-loss identification.

The ablation results further show that the effects of BN and DW are not simply additive. BN helps stabilize the propagated feature distribution during graph convolution, while DW introduces the distance-dependent spatial relationship between sensor nodes and bolt nodes into the graph structure. When the two strategies are combined, the model achieves improved prediction accuracy and more stable prediction performance. This indicates that BN and DW play complementary roles in feature propagation and spatial relationship representation for multi-sensor EMI-based bolt preload-loss prediction.

Although the proposed GCN-BN-DW model shows improved prediction performance for the present four-bolt connection structure, several limitations should be noted. First, the experimental validation was conducted on a specific bolt connection configuration under relatively stable laboratory conditions, and the generalization ability of the model for different structural forms, bolt numbers, sensor layouts, and boundary conditions still requires further investigation. Therefore, the trained model and the distance-weighted adjacency matrix should not be directly transferred to a new structure without recalibration. For a different bolted structure, the graph topology, sensor–bolt distance matrix, feature extraction range, and model parameters should be updated using representative experimental data. Second, the available EMI dataset is relatively limited, and the model performance may be affected by environmental factors such as temperature variation, sensor installation quality, and measurement noise. Future work will focus on expanding the experimental dataset, introducing independent test structures, and evaluating the robustness of the proposed graph-based model under more complex engineering conditions. In addition, incorporating physical constraints or physics-informed learning strategies may further improve the interpretability and generalization capability of the model.

Author Contributions: Conceptualization, L.L. and Y.W.; methodology, L.L. and Y.W.; software, L.L.; validation, L.L. and Y.W.; formal analysis, L.L.; investigation, L.L. and Y.W.; resources, X.F., T.Z. and J.M.; data curation, L.L. and Y.W.; writing—original draft preparation, L.L.; writing—review and editing, X.F., T.Z. and J.M.; visualization, L.L.; supervision, X.F., T.Z. and J.M.; project administration, X.F. and J.M.; funding acquisition, X.F. and J.M. All authors have read and agreed to the published version of the manuscript.

Funding: This research was funded by the Natural Science Basic Research Program of Shaanxi, grant number 2025JC-YBMS-088; and the QinChuangYuan Platform High-level Innovation and Entrepreneurship Talent Projects, grant number QCYRCXM-2022-311.

Data Availability Statement: All original simulation data, mesh files, and model parameter files involved in this study can be provided upon reasonable request to the corresponding author.

Acknowledgments: The authors gratefully acknowledge the financial support provided by the above-mentioned funding projects.

Conflicts of Interest: Author Xingyu Fan was employed by the company Zhejiang Zomax Transmission Co., Ltd. The remaining authors declare that the research was conducted in the absence of any commercial or financial relationships that could be construed as a potential conflict of interest.

References

1. An, Q.; Wang, C.; Ma, T.; Zou, F.; Fan, Z.; Zhou, E.; Ge, E.; Chen, M. Aeronautical composite/metal bolted joint and its mechanical properties: A review. *J. Intell. Manuf. Spec. Equip.* **2024**, *5*, 70–91. [CrossRef]
2. Yuan, D.; Wan, Q.; Wang, D. Influence of bolt preload degradation on nonlinear vibration responses of jointed structures. *J. Sound Vib.* **2025**, *595*, 118797. [CrossRef]
3. Miao, R.; Shen, R.; Zhang, S.; Xue, S. A review of bolt tightening force measurement and loosening detection. *Sensors* **2020**, *20*, 3165. [CrossRef] [PubMed]
4. Wang, F.; Song, G. Bolt early looseness monitoring using modified vibro-acoustic modulation by time-reversal. *Mech. Syst. Signal Process.* **2019**, *130*, 349–360. [CrossRef]

5. Yu, H.; Guo, C.; Li, N.; Lu, S. Research on bolt looseness monitoring based on electromechanical impedance transmissibility technology. *Smart Mater. Struct.* **2023**, *32*, 095009. [CrossRef]
6. Chen, D.; Huo, L.; Song, G. EMI based multi-bolt looseness detection using series/parallel multi-sensing technique. *Smart Struct. Syst.* **2020**, *25*, 423–432.
7. Huo, L.; Chen, D.; Liang, Y.; Li, H.; Feng, X.; Song, G. Impedance based bolt pre-load monitoring using piezoceramic smart washer. *Smart Mater. Struct.* **2017**, *26*, 057004. [CrossRef]
8. Wu, J.; Chen, Y.; Wang, J.; Liu, Z.; Li, W. Electromechanical impedance instrumented wearable piezoelectric ring-type sensor for bolted connection monitoring. *IEEE Sens. J.* **2023**, *23*, 14872–14881. [CrossRef]
9. Moharana, S.; Sevugaperumal Arun, V. Piezo impedance-based monitoring of loosening of bolts: Experimental and numerical study. *J. Intell. Mater. Syst. Struct.* **2022**, *33*, 1056–1071.
10. Chen, Y.; Lin, W.; Chen, H.; Du, Y.; Wei, J. Automatic detection method for loose bolts in steel frame structures based on wearable lightweight impedance system and multi-channel information fusion deep learning model. *Struct. Health Monit.* **2025**, 14759217251353110. [CrossRef]
11. Jiang, Y.Z.; Zhang, Y.B.; Zeng, L.Y.; Huang, L.; Su, B.W.; Chen, L.C. A new magnetic method for monitoring the tightness of bolted flanged connection. *Measurement* **2025**, *258*, 119434. [CrossRef]
12. Chen, G.; Shao, W.; Liu, Q.; Sun, H.; Huo, S.; Fu, H.; Qing, X. A Generalized Zero-Shot Regression Framework for Cross-Domain Damage Identification in Composite Structures. *IEEE Trans. Ind. Inform.* **2026**, *22*, 6164–6175. [CrossRef]
13. Yuan, R.; Lv, Y.; Kong, Q.; Song, G. Percussion-based bolt looseness monitoring using intrinsic multiscale entropy analysis and BP neural network. *Smart Mater. Struct.* **2019**, *28*, 125001. [CrossRef]
14. Li, X.X.; Li, D.; Ren, W.X.; Zhang, J.S. Loosening identification of multi-bolt connections based on wavelet transform and ResNet-50 convolutional neural network. *Sensors* **2022**, *22*, 6825. [CrossRef] [PubMed]
15. Yuan, C.; Wang, S.; Qi, Y.; Kong, Q. Automated structural bolt looseness detection using deep learning-based prediction model. *Struct. Control Health Monit.* **2022**, *29*, e2899.
16. Na, W.S. Bolt loosening detection using impedance based non-destructive method and probabilistic neural network technique with minimal training data. *Eng. Struct.* **2021**, *226*, 111228. [CrossRef]
17. Liu, P.; Wang, X.; Chen, T.; Wang, Y.; Mao, F.; Liu, W. Research on a percussion-based bolt looseness identification method based on phase feature and convolutional neural network. *Smart Mater. Struct.* **2023**, *32*, 035010. [CrossRef]
18. Na, W.S. A portable bolt-loosening detection system with piezoelectric-based nondestructive method and artificial neural networks. *Struct. Health Monit.* **2022**, *21*, 683–694.
19. Meher, U.; Mishra, S.K.; Sunny, M.R. Impedance-based looseness detection of bolted joints using artificial neural network: An experimental study. *Struct. Control Health Monit.* **2022**, *29*, e3049. [CrossRef]
20. Scarselli, F.; Gori, M.; Tsoi, A.C.; Hagenbuchner, M.; Monfardini, G. The graph neural network model. *IEEE Trans. Neural Netw.* **2008**, *20*, 61–80. [CrossRef] [PubMed]
21. Zhang, S.; Tong, H.; Xu, J.; Maciejewski, R. Graph convolutional networks: A comprehensive review. *Comput. Soc. Netw.* **2019**, *6*, 11. [CrossRef] [PubMed]
22. Zhou, L.; Chen, S.X.; Ni, Y.Q.; Choy, A.W.H. EMI-GCN: A hybrid model for real-time monitoring of multiple bolt looseness using electromechanical impedance and graph convolutional networks. *Smart Mater. Struct.* **2021**, *30*, 035032. [CrossRef]
23. Tang, L.; Lu, H.; Pang, Z.; Li, Z.; Su, J. A distance weighted linear regression classifier based on optimized distance calculating approach for face recognition. *Multimed. Tools Appl.* **2019**, *78*, 32485–32501. [CrossRef]
24. Bjorck, J.; Gomes, C.P.; Selman, B.; Weinberger, K.Q. Understanding batch normalization. *Adv. Neural Inf. Process. Syst.* **2018**, *31*, 7705–7716.
25. Na, W.S.; Baek, J. A review of the piezoelectric electromechanical impedance based structural health monitoring technique for engineering structures. *Sensors* **2018**, *18*, 1307. [CrossRef] [PubMed]
26. Asuero, A.G.; Sayago, A.; González, A. The correlation coefficient: An overview. *Crit. Rev. Anal. Chem.* **2006**, *36*, 41–59. [CrossRef]
27. Xu, J.; Dong, J.; Li, H.; Zhang, C.; Ho, S.C. Looseness monitoring of bolted spherical joint connection using electro-mechanical impedance technique and BP neural networks. *Sensors* **2019**, *19*, 1906. [CrossRef] [PubMed]
28. Garbin, C.; Zhu, X.; Marques, O. Dropout vs. batch normalization: An empirical study of their impact to deep learning. *Multimed. Tools Appl.* **2020**, *79*, 12777–12815. [CrossRef]
29. Ioffe, S.; Szegedy, C. Batch normalization: Accelerating deep network training by reducing internal covariate shift. In Proceedings of the International Conference on Machine Learning, PMLR, Lille, France, 7–9 July 2015; pp. 448–456.

Disclaimer/Publisher's Note: The statements, opinions and data contained in all publications are solely those of the individual author(s) and contributor(s) and not of MDPI and/or the editor(s). MDPI and/or the editor(s) disclaim responsibility for any injury to people or property resulting from any ideas, methods, instructions or products referred to in the content.